

Numerical simulation of cylindrical heat pipe considering non-Darcian transport for liquid flow inside wick and mass flow rate at liquid-vapor interface

N. Pooyoo ^{a,*}, S. Kumar ^a, J. Charoensuk ^b, A. Suksangpanomrung ^c

^a Energy Field of Study, School of Environment, Resources and Development, Asian Institute of Technology, Klong Luang, Pathumthani 12120, Thailand

^b Faculty of Engineering, King Mongkut Institute of Technology Ladkrabang, Ladkrabang, Bangkok 10520, Thailand

^c Department of Mechanical Engineering, Academic Division, Chulachomklao Royal Military Academy, Maung, Nakorn-Nayok 26001, Thailand



ARTICLE INFO

Article history:

Received 26 November 2012

Received in revised form 8 September 2013

Accepted 9 November 2013

Available online 21 December 2013

Keywords:

Cylindrical heat pipe

Non-Darcian transport

Porous wick

Finite volume method

ABSTRACT

Simulation of a copper cylindrical heat pipe was carried out assuming steady state laminar flow, incompressible flow in liquid-wick and ideal gas incompressible flow in vapor section in three dimensions to estimate the temperature, pressure and velocity profiles. The model used non-Darcian transport through porous wick to determine liquid flow in liquid-wick section. The mass flow rate describes the fluid flow at liquid-vapor interface instead of conjugate heat transfer problem. Heat source of evaporation and condensation was considered in the total enthalpy equation of liquid-wick section to describe the loss and gain of heat from evaporation and condensation. The non-linear algebraic equations from finite volume method discretization were solved by iterative segregation method and the SIMPLEC algorithm. The numerical results of axial outer wall temperature, centerline pressure and velocity magnitude were found to be in good agreement with cylindrical heat pipe operation. The results of axial outer wall temperature and velocity magnitude streamlines are better than the results obtained in earlier studies and the results of axial outer wall temperature are in a good agreement with experimental results. The hypotheses test by two-sample *t*-test method between the numerical results and experimental results for axial outer wall temperature shows that they are not statistically different.

© 2013 Elsevier Ltd. All rights reserved.

1. Introduction

Heat pipes transfer heat with small difference in temperatures between heat input and heat output, and at a high effective thermal conductivity [1]. As shown in Fig. 1 [2], conventional heat pipes have structures which consist of evaporation, adiabatic (transport) and condensation section. The heat is transferred to the evaporation zone by conduction through the pipe wall and wick structure, and vaporizes the working fluid. The vapor pressure then drives the vapor through the adiabatic zone to the condenser zone. At condenser, the vapor condenses and releases its latent heat of vaporization to the heat sink. The capillary pressure created by the wick structure pumps the condensed fluid back to the evaporator. Thus, the heat pipe can continuously transport the latent heat of vaporization from the evaporator to the condenser. This process will continue as long as there is sufficient capillary pressure to drive the condensate back to the evaporator.

The system geometry depends on the type heat pipe applications. The five major types of heat pipes are tubular including individual micro heat pipe, flat plate including vapor chambers, micro heat pipe and arrays, loop heat pipes and direct contact system [3]. The cross sections of tubular heat pipes are mostly round, oval and rectangular [3]. The tubular geometry with round cross section, considered as cylindrical heat pipes has two prime functions – heat transfer to remote location and production of compact heat sink [3]. They are suitable for applications in electronics cooling, die casting and injection moulding, heat recovery and other energy conserving uses, de-icing duties, cooking, control of manufacturing process temperature, thermal management of space craft and in renewable energy systems, but other geometries can be adopted to meet special requirements [3]. Studies to assess their performance through thermal resistance or a drop of temperature gradient along their axial distance and focusing on axial pressure and velocity magnitude to present physical principle of cylindrical heat pipe operation have been conducted by many researchers using different assumptions as follows [4–17].

* Corresponding author. Tel.: +66 2 524 5407; fax: +66 2 524 5439.

E-mail addresses: narong.pooyoo@ait.ac.th, pooyoonarong101@gmail.com (N. Pooyoo).

Nomenclature

Evaporation and condensation at liquid-vapor interface have been described using the conjugate heat transfer problem [4,13,15], liquid-vapor coupling with interfacial velocity [5,6], and liquid-vapor coupling with uniform radial blowing and suction velocities [7-12]. The liquid flows through porous wick are presented using different numerical model were the generalized Navier-Stokes equations [4], Darcy's law [5,6,9,10,13-15], non-Darcian transport (Brinkman) [12,16] and non-Darcian transport (Brinkman and Forcheiner) [7,15]. The pure conduction heat transfer has been used to describe heat transfer in liquid-wick region

[4,16,17], and the effective thermal conductivity of saturated wick considering liquid flow to describe heat transfer in liquid-wick region [9,10,13,15].

These above studies used different assumptions to predict thermal resistance or axial temperature gradient, centerline pressure, velocity magnitude, and there are gaps in these numerical models for cylindrical heat pipes. These gaps are due to the use of generalized Navier–Stokes equation ignoring fluid inertia and the drag force exerted by the liquid on the solid. However, non-Darcian transport (Brinkman and Forchheimer) with analytical solution

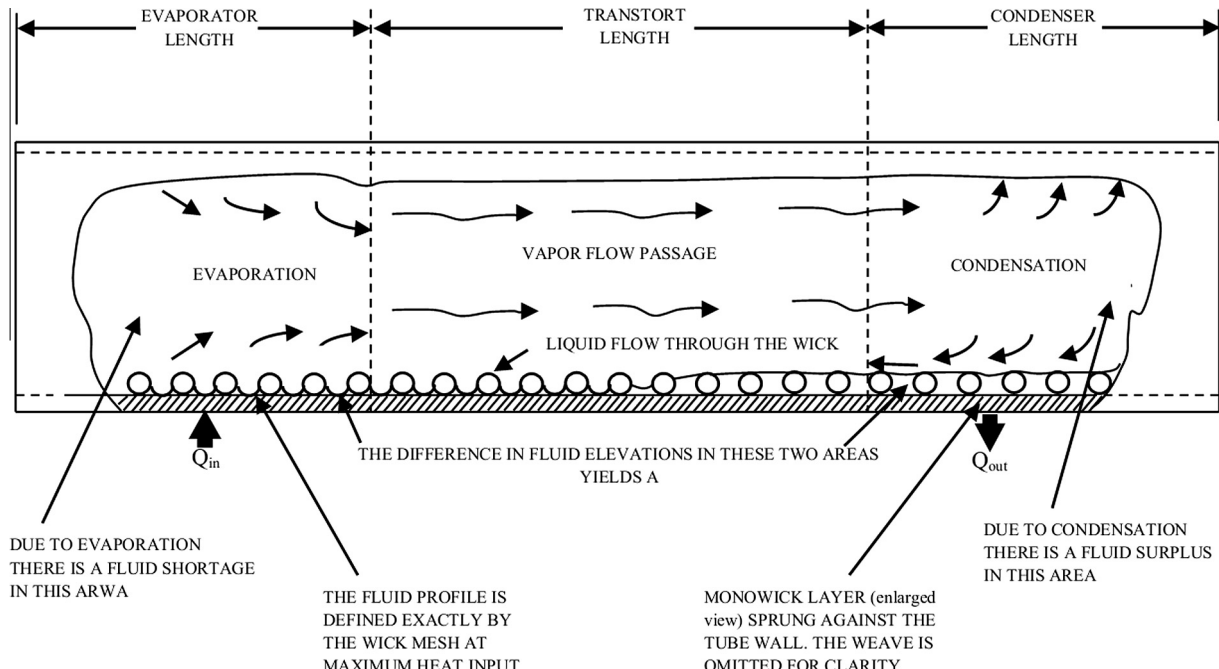


Fig. 1. Principle of operation of cylindrical heat pipe [2].

shows that the vapor and liquid pressure distributions and the centerline vapor velocities compare very well with both experimental and numerical results [7] and currently, other non-Darcian transport (Wang and Cheng) has been used in Computational Fluid Dynamic (CFD) software [18]. The numerical model ignoring liquid flow inside the wick leads to inaccurate estimation of the temperature field [15]. Thus, using pure conduction is not suitable. The evaporation and condensation occur at liquid-wick zone results in loss and gain of heat, and thus, the modeler should add evaporation and condensation heat source to the total enthalpy equation of liquid-wick zone [9,16]. Conjugate heat transfer problem with heat conduction in a solid region is closely coupled with convection heat transfer in an adjacent fluid region [19] and is not suitable for simulation to describe fluid flow at liquid-vapor interface because this model needs to be simulated under wall boundary condition. This condition causes difficulties to show fluid flow and flow direction at liquid-vapor region. Besides, liquid-vapor coupling without inflow and outflow mass flow rate model also causes difficulties to simulate recirculation of cooling agent in cylindrical heat pipes.

Thus, in this work, a new numerical model for simulation of cylindrical heat pipe has been proposed and developed by addressing these research gaps. The proposed model is non-Darcian transport (Wang and Cheng) incorporated with the mass flow rate conditions, non-pure conduction heat transfer at liquid-wick region and adding heat source of evaporation and condensation into liquid-wick zone. The non-Darcian transport (Wang and Cheng) [20] is employed to determine liquid flow through porous wick. The mass flow rate is used to determine mass flow rate per radian across liquid-vapor interface resulting in evaporation and condensation instead of conjugated heat transfer problem. The non-pure conduction heat transfer is used to determine conduction and convection heat transfer in the liquid-wick region and the heat source is added to the total enthalpy equation in liquid-wick region to simulate the loss and gain of latent heat of evaporation and condensation at liquid-vapor interface. The numerical results on the axial outer wall temperature including thermal resistance, centerline pressure, centerline velocity magnitude and velocity

magnitude vector were then compared with those obtained from previous studies [4,15]. The governing equations are used to obtain these outputs consisting of continuity equation, Navier-Stokes equations with extending of Wang and Cheng [20] called non-Darcian transport (Wang and Cheng), and the total enthalpy equations to present temperature of the entire computational domains of cylindrical heat pipe. The governing equations of the proposed model are discretized by finite volume method to obtain the algebraic equations, and these are solved by iterative segregated method and adopting Simi-Implicit Method Pressure Link Equation-Consistent (SIMPLEC) algorithm [18].

2. Governing equations

The finite volume method is used to solve fluid flow and heat transfer of cylindrical heat pipe. This method begins with governing equations of the proposed model and discretization of the governing equations to the algebraic equation. The governing equations in this study are Navier-Stokes equations by extended Wang and Cheng, generalized Navier-Stokes equations, total enthalpy equations and the continuity equation is used to present mass flow rate flow through liquid-vapor interface. The following presents details of these governing equations and related equations in cylindrical coordinates and velocity components (v, u, w) for r, θ, z directions, respectively:

2.1. Liquid-wick region

The liquid flow through porous wick (liquid-wick region) was simulated using the Navier-Stokes equations by extended of Wang and Cheng's equations using the following assumptions:

- Since cylindrical heat pipes operate with non-uniform heat input [15], 3D analysis was considered for this study [4,15].
- Steady state laminar flow was assumed [4–15,17].
- Incompressible flow inside liquid-wick region [4–15,17].
- Considered non-Darcian transport (Wang and Cheng).
- Cooling agent as Newtonian fluid [4–15,17].

- State of boiling of the working fluid is not reached for this model [4–15,17].
- Gravity effect is ignored as the analysis is for horizontal cylindrical heat pipe [4–17].

The compact vector notation form can be written as follows [18]:

$$\nabla \cdot (\rho_l \varepsilon \vec{V} \vec{V}) = -\varepsilon \nabla P + \nabla \cdot (\varepsilon \tau) - \frac{\mu_l \varepsilon^2 \vec{V}}{K} - \frac{\varepsilon^3 \rho_l C_F}{\sqrt{K}} |\vec{V}| \vec{V} \quad (1)$$

The first term is the convection term. The second and third terms are pressure and viscous force terms. The last two terms represent the additional drag force imposed by the pore walls on the fluid inside pores (and usually results in a significant pressure drop across the porous solid). The C_F can be calculated from [21],

$$C_F = \frac{1.75}{\sqrt{150\varepsilon^3}} \quad (2)$$

The porosity presents the volume occupied by the pores to the total volume of the porous solid, while permeability is a quantity representing the surface area to volume ratio of the porous matrix [18]. The permeability of screen wick structures for this study is presented the following equation [22].

$$\frac{d_w^2 \varepsilon^3}{122(1-\varepsilon)^2} \quad (3)$$

$$\varepsilon = 1 - \left(\frac{1.05\pi N d_w}{4} \right) \quad (3.a)$$

2.2. Liquid–vapor interface

The liquid and vapor phases are coupled at the liquid–vapor interface and the mass balance equation is used to describe the phase transition at liquid–vapor interface. The mass balance equation in the r -direction at the liquid–vapor interface yields the following equation:

$$\rho_l A_i v_l = \rho_v A_i v_v \quad (4)$$

This can be used to predict the blowing velocity and suction velocity using the relationships among velocity magnitude, heat input, at liquid–vapor interface, surface area of liquid–vapor interface and latent heat of evaporation and condensation at liquid–vapor interface as follows [7–12]:

$$Q_i = m_i h_{fg} = \rho_v A_i V_i h_{fg} \quad (5)$$

$$V_{i,e} = -\frac{Q_{i,e}}{2\pi R_i L_e \rho_v h_{fg}} \quad (6)$$

$$V_{i,a} = 0 \quad (7)$$

$$V_{i,c} = +\frac{Q_{i,c}}{2\pi R_i L_c \rho_v h_{fg}} \quad (8)$$

These velocity equations provide additional details to determine the mass flow rate per radian to apply into inlet boundary condition at liquid–vapor interface for evaporator, adiabatic section and condenser, instead of conjugate heat transfer problem, as follows:

$$m_{i,e} = -[\rho_v (2\pi R_i L_e) V_{i,e}] / 2\pi \quad (9)$$

$$m_{i,a} = 0 \quad (10)$$

$$m_{i,c} = +[\rho_v (2\pi R_i L_c) V_{i,c}] / 2\pi \quad (11)$$

The negative sign refers to outflow liquid–wick region and the positive sign for inflow liquid–wick region.

2.3. Vapor region

The generalized Navier–Stokes equations to simulate the vapor flow inside vapor region uses the following assumptions:

- Most cylindrical heat pipe operates with non-uniform heat input [15]. Thus, a 3D approach is more suitable for the numerical simulation [4,15].
- Steady state laminar flow [4–15,17].
- Ideal gas incompressible flow inside vapor region [4,15].
- Working fluid as Newtonian fluid [4–15,17].
- The cylindrical heat pipe for this study is low temperature heat pipes. Thus, uniform vapor temperature is used for the numerical simulation [7].
- Gravity effect is ignored because of horizontal cylindrical heat pipe position [4–15,17].

These assumptions help to formulate the generalized Navier–Stoke equations in compact vector notation form in the vapor region as follows [18,23]:

$$\nabla \cdot (\rho_v \vec{V} \vec{V}) = -\nabla P + \nabla \cdot (\tau) \quad (12)$$

The first term is the convection term. The second and third terms are pressure and viscous force terms. The vapor density is calculated by using the ideal gas equation as follows:

$$P_v = \rho_v R T_v \quad (13)$$

2.4. Total enthalpy equation

The total enthalpy equation is used to indicate heat transfer in whole domains of the cylindrical heat pipe. The details of total enthalpy equation in liquid–wick region, vapor region and cylindrical heat pipe container are presented as follows:

2.4.1. Liquid–wick region

The compact vector notation of the total enthalpy equation to obtain the temperature profile inside liquid–wick region of cylindrical heat pipe is [18,23]:

$$\nabla \cdot (\rho_l \varepsilon \vec{V} h_0) = \nabla \cdot (k_{eff} \Delta T) + (\varepsilon \tau) : \nabla \vec{V} + \varepsilon \frac{\partial p}{\partial t} + S_h \quad (14)$$

$$h_0 = i + \frac{p}{\rho_l} + \frac{1}{2}(u^2 + v^2 + w^2) \quad (14.a)$$

The first term in Eq. (14) is the total enthalpy term resulting in the rate of change of energy of a fluid particle related to porosity. The second term is the rate of heat addition to the fluid particle due to heat conduction, which is presented by Laplacian equations. The third term gives the rate of work done on the particle by surface stresses related to porosity. The fourth term is the rate of change of pressure related to porosity and the last term is the specific total enthalpy source term resulting in evaporation and condensation at liquid–vapor interface.

The k_{eff} represents the effective thermal conductivity for heat conduction at liquid-saturated wick structures [24] and S_h refers to the added total enthalpy source term to determine the evaporation and condensation at liquid–vapor interface. The effective thermal conductivity of screen wick can be calculated using information given in the following equation [24].

$$\frac{k_l[(k_l + k_w) - (1 - \varepsilon)(k_l - k_w)]}{(k_l + k_w) + (1 - \varepsilon)(k_l - k_w)} \quad (15)$$

The source term is formulated by total heat input and total heat output per volume of liquid-vapor interface. The source terms for vaporization in evaporator, adiabatic section and condenser is given by the following equations [9]:

$$S_e = -\frac{\dot{Q}_{i,e}}{\pi((R_i + t_w)^2 - R_i^2)L_e} \quad (16)$$

$$S_a = 0 \quad (17)$$

$$S_c = +\frac{\dot{Q}_{i,c}}{\pi((R_i + t_w)^2 - R_i^2)L_c} \quad (18)$$

The negative sign refers to heat loss in evaporator liquid-wick region resulting from evaporation at liquid-vapor interface, and the positive sign refers to heat received in condenser liquid-wick region from condensation at liquid-vapor interface.

2.4.2. Vapor region

The compact vector notation of the total enthalpy equation to obtain temperature profile inside vapor core of cylindrical heat pipe is given as follows [18,23]:

$$\nabla \cdot (\rho_v \vec{V} h_0) = \nabla \cdot (k_v \Delta T) + (\tau) : \nabla \vec{V} + \frac{\partial p}{\partial t} \quad (19)$$

This equation is similar to Eq. (14) except that this equation omits the source term for evaporation, condensation, and the porosity of screen wick.

2.4.3. Cylindrical heat pipe container

The total enthalpy equation omitting convection, viscous and pressure term is used to determine heat transfer through cylindrical heat pipe container. The total enthalpy equation assuming 3D steady state thermal conduction is obtained from the following equation [18,23]:

$$\nabla \cdot (k_s \Delta T) = 0 \quad (20)$$

3. Cylindrical heat pipe geometry and computational domains

The numerical simulation was conducted by using commercial software from Computational Fluid Dynamic Research Cooperation (CFD-RC) of ESI group. Three programs used for the numerical simulation are CFD-GEOM, CFD-ACE+ and CFD-VIEW. The numerical simulation begins with geometry and grid generation (pre-process) by using CFD-GEOM. Then, the complete pre-process was solved by using CFD-ACE+(solver process) and output presented by using CFD-VIEW (post-process). For the pre-process, the details of geometry and grid generation are as follows.

The geometry of water-copper cylindrical heat pipe for this study has the following dimensions: 1000 mm length, 10 mm of evaporator endcap, 24 mm of condenser endcap, 25.4 mm outer diameter, 0.85 mm wall thickness, 0.356 mm wick thickness. The evaporator, adiabatic and condenser lengths are 64, 606, and 296 mm, respectively as shown in Fig. 2a. Heat flux transfers to evaporator and transfers from condenser to surrounding by circumferential heat (uniform heat in circumferential direction and heat transfer direction refer to arrow sign as shown in Fig. 2a). This geometry is changed into the three dimensions of one segment geometry in r , θ , z coordinates. This geometry is divided into three sections consisting of evaporator (B), adiabatic section (C) and condenser (D) as shown in Fig. 2b for use in grid generation, volume condition and boundary condition preparation in the pre-process. The volume conditions are container wall (F), liquid-wick region (G) and vapor region (H), evaporator endcap (A), condenser endcap

(E). The grid for three dimensional one segment is generated by two-dimensional grid extrusion method using CFD-GEOM program. As shown in Fig. 2c, the generated grid in r , θ , z coordinates is hexagonal structured grid and number of total nodes is 1,275,660. The grid points are $72 \times 60 \times 373$ for the radial, circumferential, axial direction, respectively.

4. Grid independence study

The accuracy and convergence of the results of numerical simulation depends on density of the grid because all numerical calculations are solved by the discretized form of the differential equation on a finite grid. The grid independence is used to indicate grid quality. It refers to a solution that no longer changes with further grid refinement [18]. In this study, the grid independent study was conducted by comparing the thermal performance of cylindrical heat pipes in two grid sizes. The two hexagonal structured grid sizes consist of $72 \times 60 \times 373$ (the present grid) and $80 \times 70 \times 427$ (the further grid refinement) for the radial, circumferential and axial direction, respectively. The thermal performance results give $0.89 \text{ }^{\circ}\text{C/W}$ in present grid and $0.88 \text{ }^{\circ}\text{C/W}$ in the further grid refinement. These results show that the grid size for this study gives the thermal performance does not change more than 1% from the further grid refinement. Thus, the grid size used in this study can be considered to be grid independent.

5. Numerical methods

The cylindrical heat pipe is solved by finite volume method. This method discretizes the governing equations and boundary conditions, and the result of discretization was solved by iterative segregated method and SIMPLEC algorithm. The details of boundary conditions, working properties and finite volume method are presented as follows:

5.1. Boundary conditions and working fluid properties

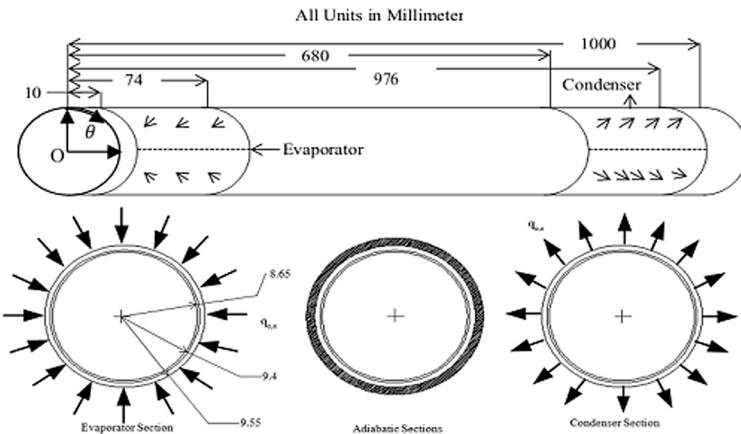
The boundary conditions and working fluid properties are input to one segment three dimensional cylindrical heat pipe grid flowing governing equations of the proposed model. The boundary conditions are assigned to boundary conditions menu and working fluid properties are assigned to volume conditions menu in CFD-ACE+ solver software. These conditions are given in Fig. 3 and Table 1.

As shown in Fig. 3a, the outer wall is assigned the boundary condition as uniform heat flux in evaporator ($+\ddot{Q}_e$) and uniform heat flux in condenser ($-\ddot{Q}_e$). These heat fluxes are estimated from

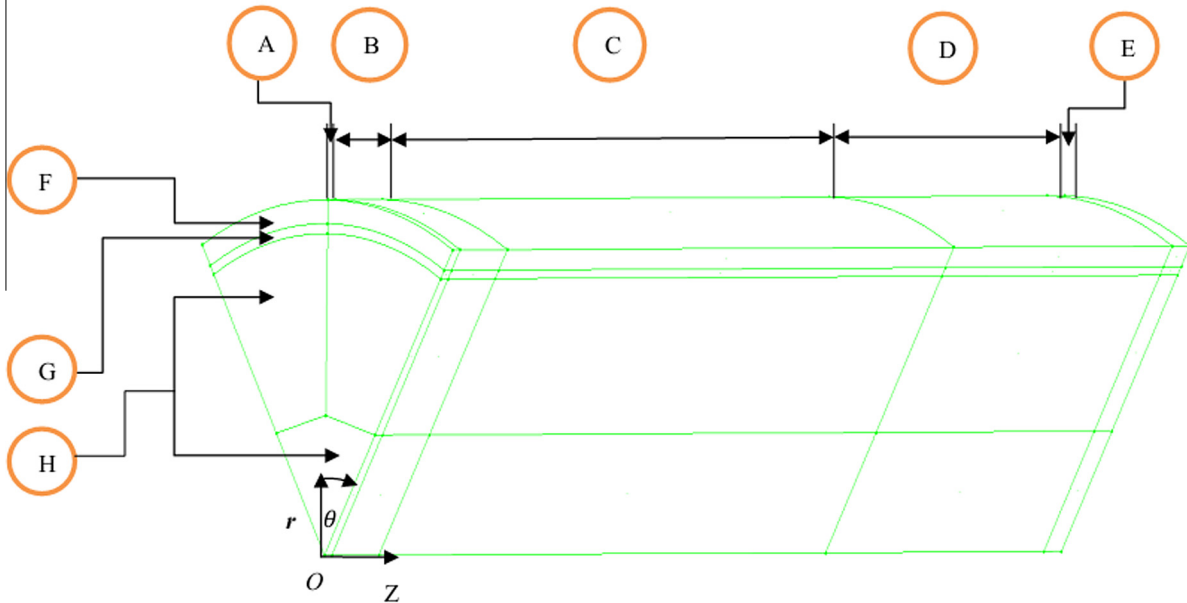
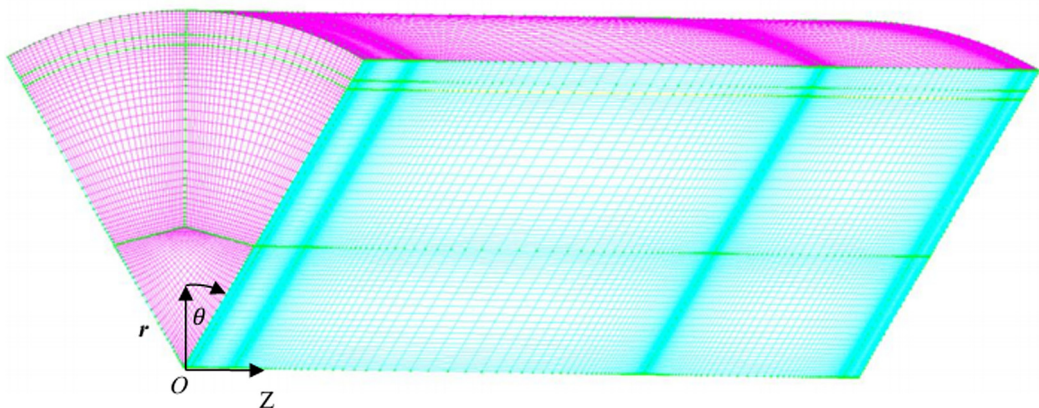
Table 1

The working fluid properties and characteristics of liquid-saturated wick structure [4].

Descriptions	Symbol and unit	Value
Saturation pressure	P_s , Pa	41,600
Saturation temperature	T_s , K	349.15
Latent heat	h_{fg} , J/kg	2,341,000
Vapor density	ρ_v , kg/m ³	0.258
Vapor dynamic viscosity	μ_v , Pa s	0.000011
Specific heat for vapor	C_v , J/kg K	1,942
Thermal conductivity of vapor	k_v , W/m K	0.0261
Liquid density	ρ_l , kg/m ³	975
Liquid dynamic viscosity	μ_l , Pa s	0.00037
Specific heat for liquid	C_l , J/kg K	4,186
Thermal conductivity of liquid	k_l , W/m K	0.0261
Wick porosity	ϵ , -	0.7
Wick permeability	K, m ²	1.3E-009
The effective thermal conductivity of wick (screen wick)	k_{eff} , W/m K	1.2

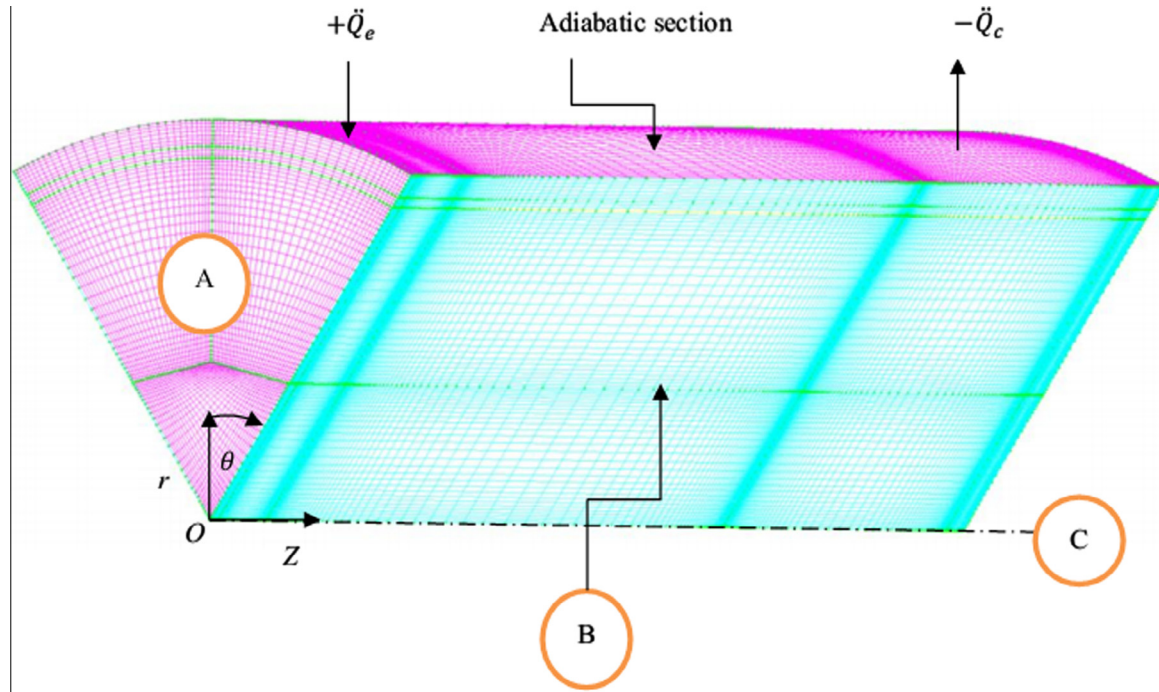


(a) Cylindrical heat pipe model used for the numerical simulation [4]

(b) 3D one segment cylindrical heat pipe geometry in r , θ , z coordinates(C) 3D one segment cylindrical heat pipe grid in r , θ , z coordinates**Fig. 2.** Cylindrical heat pipe model used for the numerical simulation [4].

100 W heat input [4] considering the surface areas of evaporator and condenser zone. The evaporator end cap (A) is assigned the adiabatic wall boundary condition and zero static pressure, while

the opposite end cap has only the adiabatic wall boundary condition. The surface (B) and its opposite side including centerline (C) are used for the symmetry boundary condition. As shown in



(a) Boundary conditions in 3D computation domains

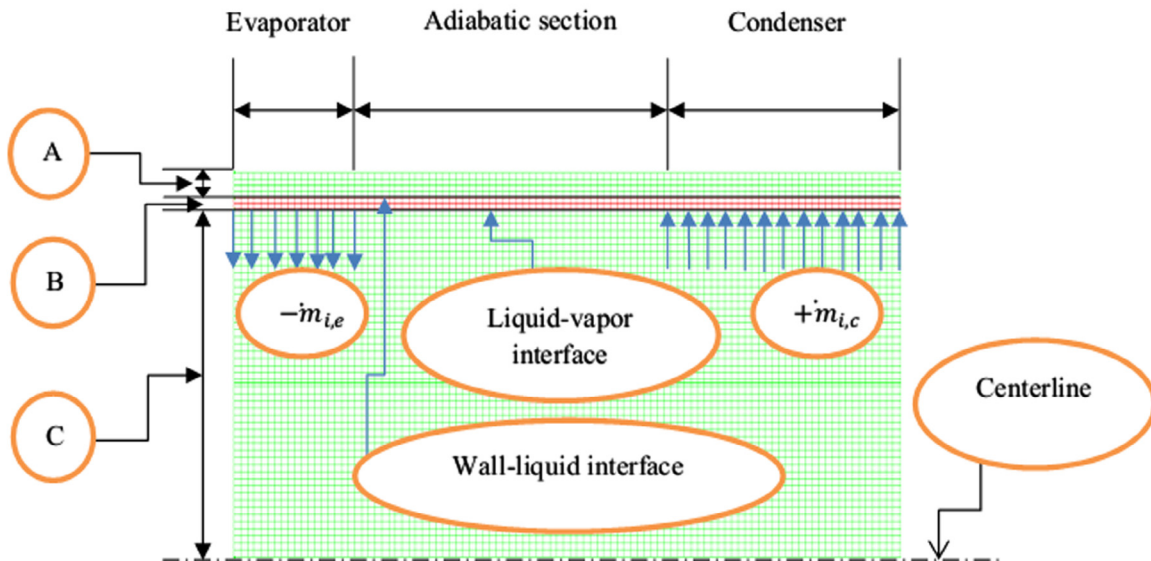


Fig. 3. Boundary conditions for the model.

Fig. 3b, the boundary conditions are used under the computational domains: container (A), liquid-wick region (B) and vapor region (C). These domains give other boundary conditions as follows.

The conjugate heat transfer problem with no-slip condition is applied to wall-liquid interface boundary condition. The outflow mass flow rate ($-m_{i,e}$) and inflow mass flow rate per radian ($+m_{i,c}$) with no-slip condition are used instead of conjugate heat transfer problem at liquid-vapor interface. These mass flow rates are calculated from uniform blowing and suction velocities [7–12] and assuming heat input at liquid–vapor interface equal to the heat input at outer surface wall [10]. Once the boundary conditions are determined, the working fluid properties at 76 °C, characteristics of screen wick and other data as shown in **Table 1** into volume conditions embedded in CFD-ACE+ solver are inputted.

5.2. Numerical conditions

The finite volume method is used to present flow and heat transfer of cylindrical heat pipes. This method begins from the governing equations discretization and their arrangement to general transport equation [18,23]. The results of general transport equation integration and application of Gauss's divergence theorem provides the usual general form of the finite difference equations in 3D steady state, laminar flow. This equation has both non-linear and linear equation forms. The convection term discretization embedded in this equation can be obtained by several schemes (first order upwind, central difference, second order upwind with limiter, smart and third order scheme). However, in this study, the second order upwind is used to obtain the interpolated value of the cell-face values in convection

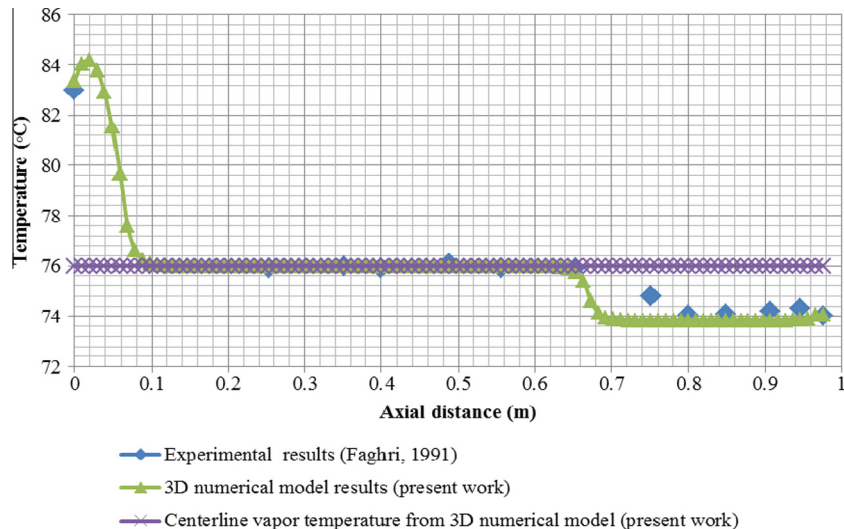


Fig. 4. The centerline vapor and the outer wall temperature distribution.

term discretization due to its good numerical accuracy and stability. An iterative segregation and the SIMPLEC algorithm are used to obtain the numerical solution for the non-linear algebraic equations. Inertial relaxation factors are determined by 0.2 in velocity and 0.02 in enthalpy and the linear relaxation factors are set up by 1 in pressure, density, viscosity, and 0.7 in temperature. The linear equations at the end of the previous iteration is solved by conjugate gradient squared (CGS) with preconditioner for velocity and enthalpy, and algebraic multigrid (AMG) solver for pressure correction. The iterations are stopped with convergence results as follows:

- The numerical simulation converges after the 22,918 iterations and 120 h.
- The residual plot for enthalpy and velocity component is four orders of magnitude drop from peak residual.
- The mass flow summary is small relative to the mass incoming value as 15 orders of magnitude ($1.77440\text{E}-05$ of inflow, $-1.77440\text{E}-05$ of outflow and $1.52466\text{E}-20$ of sum of imbalance) and total heat imbalance is not more than 1% of heat input.
- The monitor plot for temperature does not change at convergence iteration (22,918 iterations) for six significant digits (between 356.3822 and 356.3824 K).

These results guarantee that grid system, problem definition and the numerical solution for this study is valid.

6. Results and discussions

A 100 W heat input [4] which is approximate for some electronic devices is inputted to the evaporator of the copper–water cylindrical heat pipe. The numerical results considering non-Darcian transport and the mass flow rate condition using this heat input are presented as follows:

6.1. The centerline vapor and the outer wall temperature distribution

The comparison of the heat pipe outer wall temperature between present numerical results and experimental results [4] is shown in Fig. 4.

Fig. 4 shows the outer wall temperature distribution along the axial distance has the highest temperature occurring at center of evaporator and sharply drop at evaporator zone due to evaporation resulted in heat input. The uniform temperature happens along adiabatic section due to small temperature difference and the coldest happens at condenser due to condensation resulted from heat

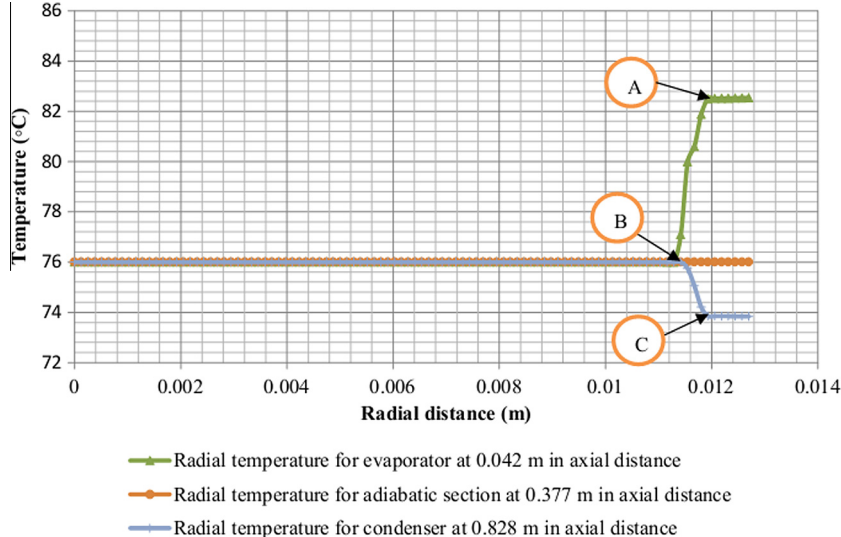


Fig. 5. The radial temperature distribution.

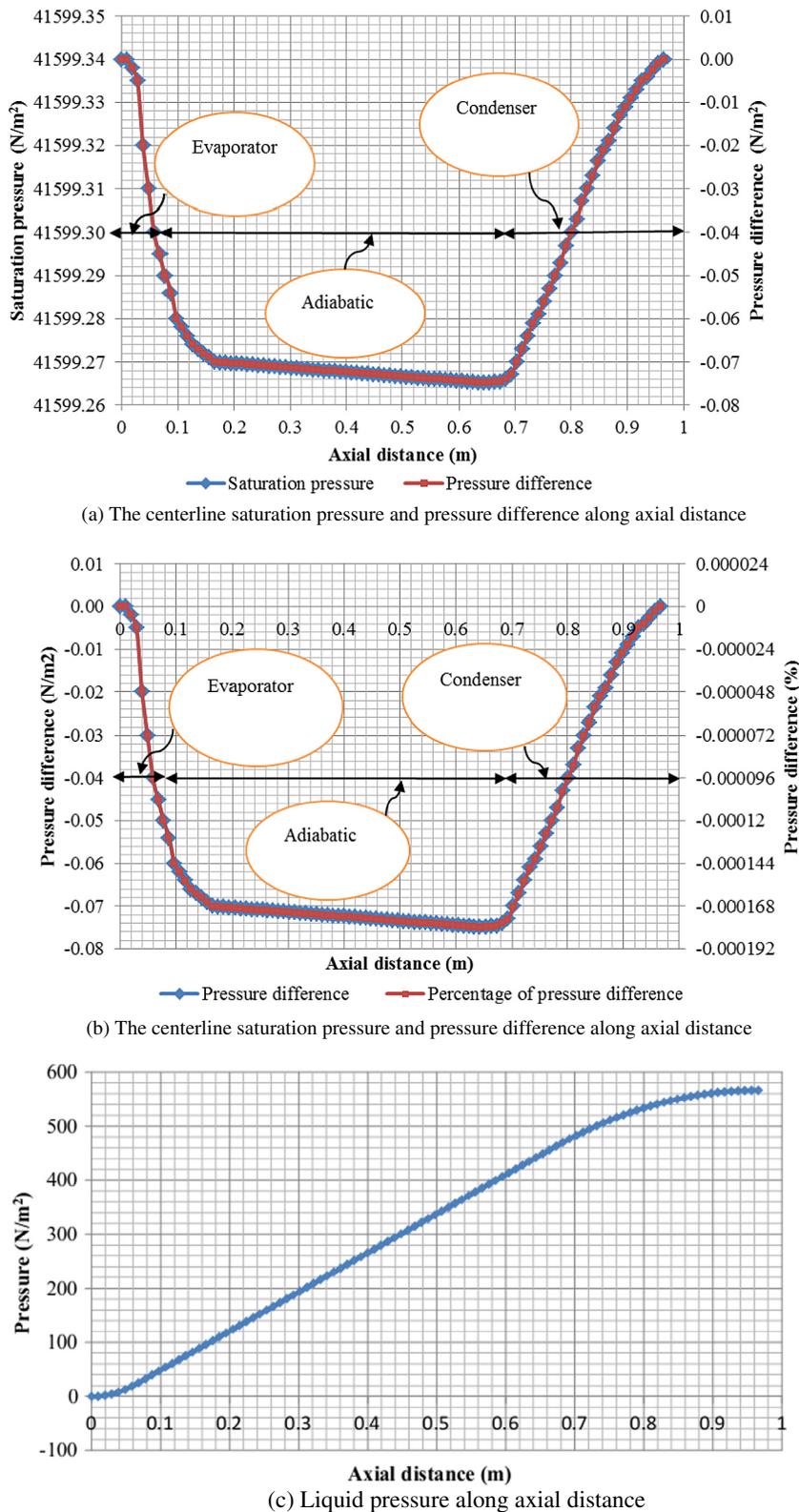
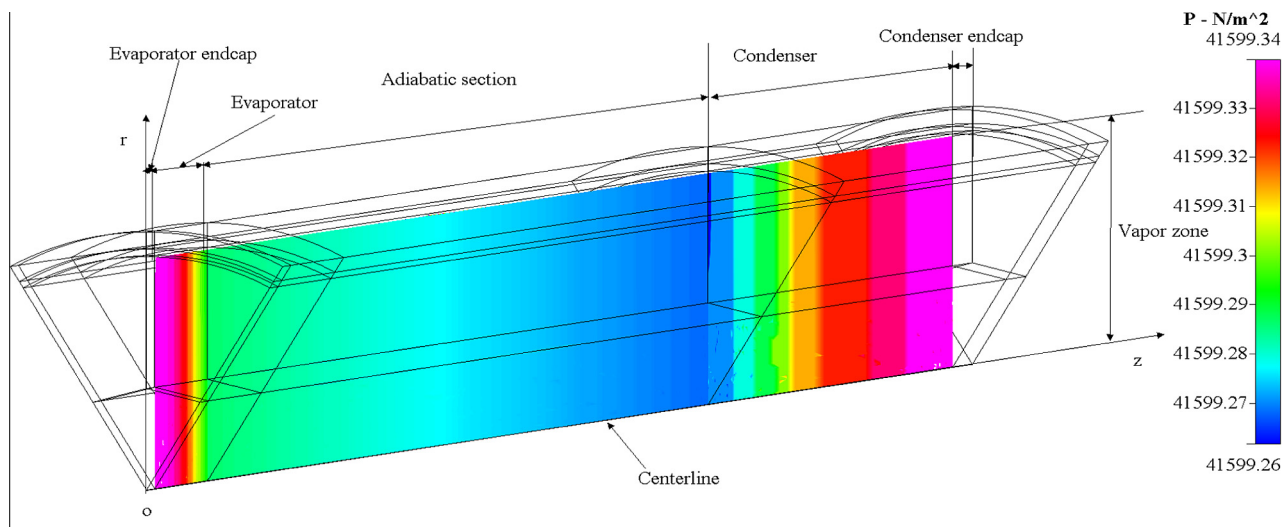
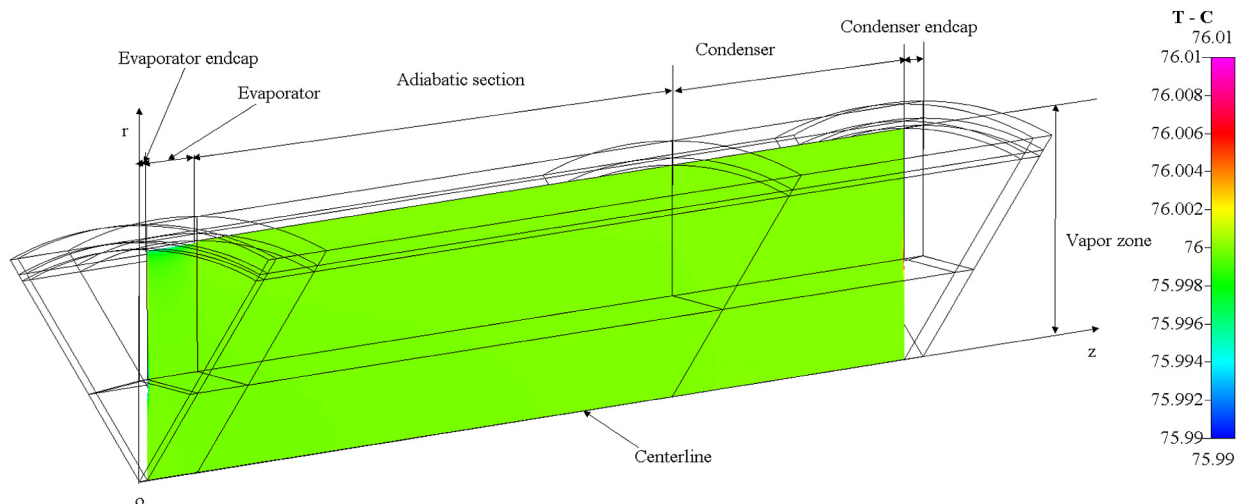
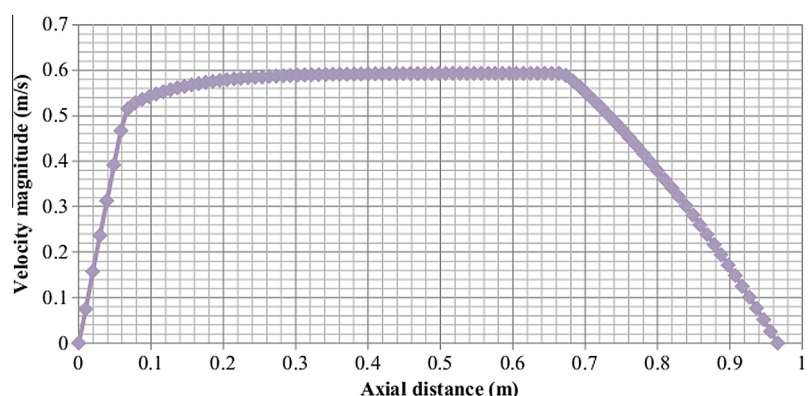


Fig. 6. The centerline pressure and liquid pressure distribution.

output. The outer wall temperature at condenser is characteristic of uniform temperature due to determine uniform heat output (non-uniform for experiment). These characteristics estimate the heat pipe performance in terms of thermal resistance ($0.89 \text{ }^{\circ}\text{C}/\text{W}$ which is in a good agreement with experimental result ($0.88 \text{ }^{\circ}\text{C}/\text{W}$) with

an error of 0.1%, and is better than numerical results of previous studies [4,15,25]. In addition, the centerline vapor temperature along axial distance has uniform temperature at saturation temperature ($76 \text{ }^{\circ}\text{C}$) due to the assumption of uniform vapor temperature for the low-temperature heat pipe [7].

(a) The contour of pressure in r - z plane(b) The contour of temperature in r - z plane**Fig. 7.** The pressure and temperature contour.**Fig. 8.** The centerline velocity magnitude distributions.

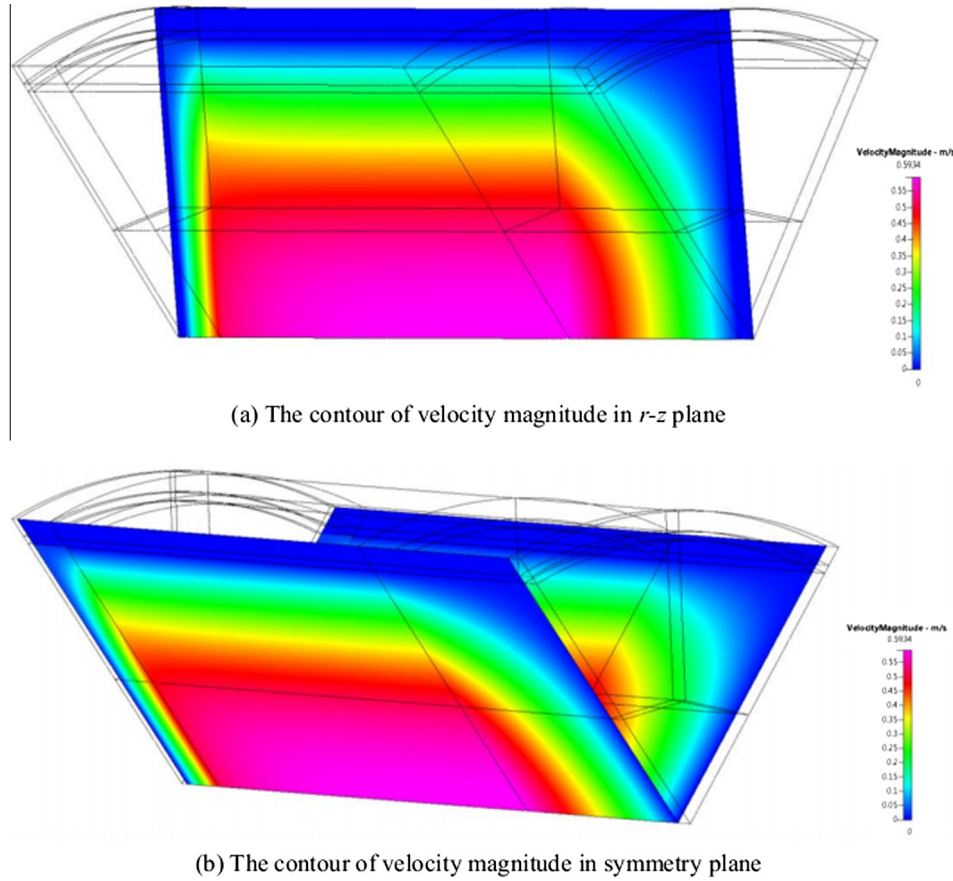


Fig. 9. The contour of velocity magnigntude.

6.2. The radial temperature distribution

The heat transfer in cylindrical heat pipe relates to thermal layer in circumferential heating. The thermal layers for cylindrical heat pipe are considered for heat pipe container, wall–liquid interface, liquid–wick, liquid–vapor interface, vapor regions and centerline. These layers have radial temperature distribution from centerline to container surface, and the results from numerical simulation are as follows:

Fig. 5 shows that the radial temperature decreases from wall–liquid interface (A) to liquid–vapor interface (B) due to heat loss in liquid–wick region to evaporate at liquid–vapor interface (B) in evaporator section. In the adiabatic section, the radial temperature from centerline to container surface are uniform at saturation temperature (76°C). In condenser section, the radial temperature decreases from liquid–vapor interface (B) to wall–liquid interface (C) due to condensation at liquid–vapor interface and heat release from liquid–wick region from the outer wall surface cooling. In addition, the radial temperatures are uniform for the heat pipe container in evaporator and condenser due to uniform heating and cooling, respectively. These are in good agreement with the results of the earlier study [14].

6.3. The results of centerline vapor and liquid pressure distribution

The centerline pressure distribution is presented in form of vapor static pressure as a function of the axial position. This variation in vapor pressure is principally the results of the viscous pressure drop occurring along the vapor flow path, and is influenced by the inertial effects resulting from the blowing and suction in the evap-

orator and condenser, respectively [24]. The centerline pressure distribution along axial distance obtained from the numerical model is shown in Fig. 6.

Fig. 6a shows the pressure difference between the saturation pressure of water at 76°C and from the governing equation for the liquid–vapor interface and vapor domain of the heat pipe. The pressure difference has been plotted with respect to the axial distance, and has been shown in terms of absolute values (difference to saturation condition) and percentage difference (Fig. 6b). The data points are the same. It can be obtained that at the evaporator zone, the static pressure decreases sharply due to blowing and vaporization at liquid–vapor interface. The static pressure at adiabatic section has a small decrease due to small difference of vapor temperature, but this static pressure difference is enough to drive the vapor flow from the evaporator through the adiabatic section to the condenser. The sharp increase occurs in the condenser zone due to pressure recovery from condensation and suction at liquid–vapor interface in condenser section. These results show good agreement with the previous study [4]. As shown in Fig. 6c, the liquid pressure drop in the liquid–wick region sharply decreases from condenser through adiabatic to evaporator sections. The liquid pressure drop is much higher than the vapor pressure drop due to use of porous media and has much different temperature in the axial distance for liquid–wick region. This result is in good agreement with the earlier studies [7,15] and the contour of pressure including temperature distribution, as shown in Fig. 7.

Fig. 7a shows that the pressure of water vapor at the vapor zone and at centerline have absolute pressure variation between $41,599.26$ and $41,599.34 \text{ N/m}^2$, and is very close to the saturation

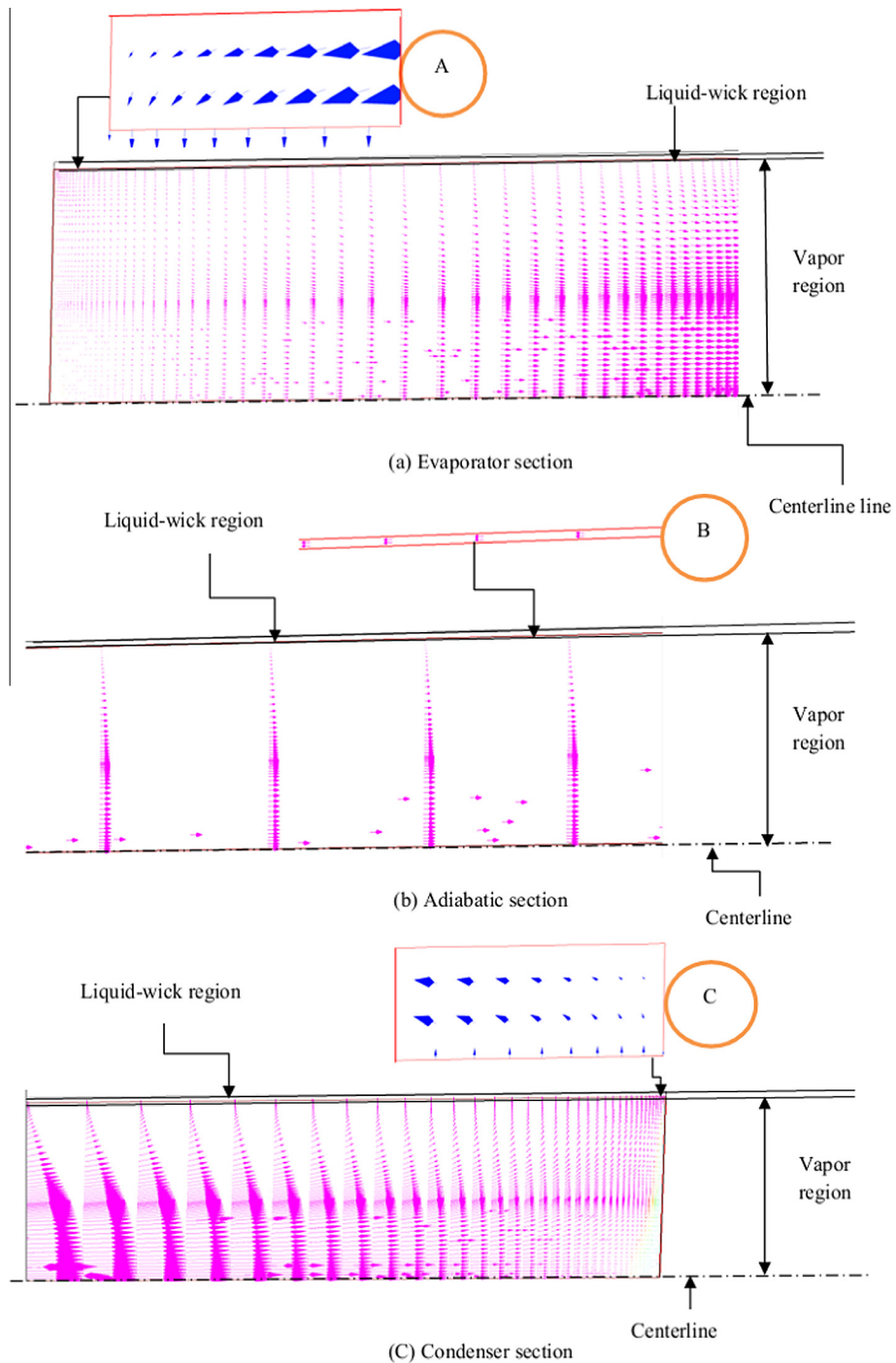


Fig. 10. The velocity vector in r - z plane.

pressure of $41,600 \text{ N/m}^2$. The contour of pressure shows very small difference at vapor zone and at centerline in r - z plane. As shown in Fig. 7b, the temperature of water vapor at vapor zone and at centerline has temperature variation between 75.99 and 76.01°C , and is very close to the saturation temperature of 76°C .

6.4. The centerline velocity magnitude distribution

The centerline velocity magnitude distribution assumes that the rates of vaporization in the evaporator and condensation in the condenser are uniform. This yields a linearly increasing value in the evaporator, and a linearly decreasing value in the condenser [24]. This relates to the numerical results as shown in Fig. 7.

Fig. 8 shows the centerline velocity magnitude from numerical results. This result presents the velocity magnitude profile. The velocity magnitude sharply increases in the evaporator zone due to vaporization, nearly uniform increases at the adiabatic section due to small temperature difference, and sharply decreases at condenser zone due to condensation. These results relate to centerline pressure distribution as shown in Fig. 6a. That is, the velocity magnitude increases when pressure is decreased and the velocity magnitude decreases when pressure is increased. This phenomenon is due to energy conservation of changing potential energy to kinetic energy. The above results are in a good agreement with previous numerical results [4], and the contour of centerline velocity magnitude in r - z plane and two symmetry planes are shown in Fig. 9.

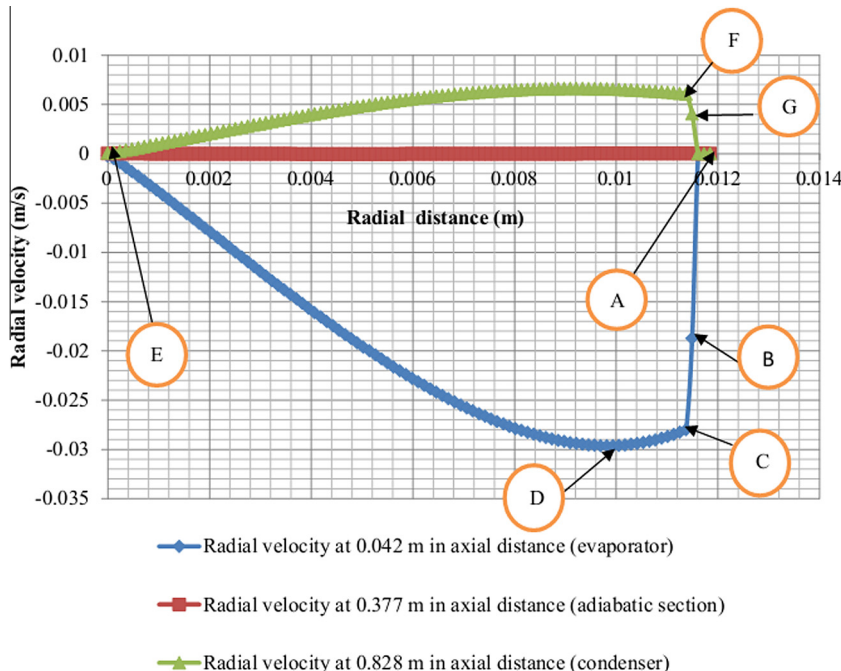


Fig. 11. The radial velocity distribution.

Fig. 8 illustrates the contour of velocity magnitude in r - z plane shown in **Fig. 9a**. The pink¹ color shows the highest velocity magnitude (occurring near centerline of cylindrical heat pipes in the adiabatic section). The velocity magnitude is linear increasing at the evaporator (from dark blue, light blue, green, yellow, red and pink color), and is linear, decreasing at the condenser (from pink, red, yellow, green, light blue to dark blue color). The velocity magnitude at the adiabatic section increases from near wall volume condition to centerline boundary condition (from dark blue, light blue, green, yellow, red and pink color). The dark blue color occurs at the wall volume condition and at the end caps of the cylindrical heat pipes (showing zero velocity magnitude). The velocity magnitude contour in r - z plane is the same as can be observed in **Fig. 9b**. Thus, the 2D-axisymmetry can be used to simulate cylindrical heat pipes instead of 3D to reduce computational resource uses. This contour gives the liquid and vapor velocity vectors in the r - z plane as shown in **Fig. 10**.

Fig. 10 shows that the velocity magnitude direction (vapor) flows from evaporator through adiabatic section to condenser and velocity magnitude direction (liquid) returns from condenser through adiabatic section to evaporator inside liquid-wick region. The liquid flows in the opposite direction of the vapor flow as shown in A, B and C. These fluid paths are in good agreement with the theoretical heat pipe operation [2], while the other previous studies [4,15] present velocity magnitude direction for vapor and liquid phase that is different from theoretical heat pipe operation [2]. This shows that the velocity magnitude direction from the present numerical model is better than the earlier numerical models [4,15].

6.5. The radial velocity distribution

The radial velocity distribution assumes that the rates of vaporization and condensation at liquid-vapor interface are uniform. This yields significant increases of radial velocity in the evaporator due to evaporation, and significant decreases of radial velocity in the condenser due to condensation (**Fig. 11**).

¹ For interpretation of color in Fig. 9, the reader is referred to the web version of this article.

It can also be observed that the radial velocity in evaporator has the outflow direction (negative sign) from wall-liquid interface (A) through liquid-vapor interface (B), near liquid-vapor interface (C), and the maximum radial velocity (D) at 0.03 m/s to centerline (E). This path shows the radial velocity increase in two stages. The first stage is the increase from wall-liquid interface (A) to liquid-vapor interface (B) due to heat storage in wick structure. The second stage is the increase from liquid-vapor interface (B) to near liquid-vapor interface (C) due to evaporation. Then, radial velocity decreases in unheated zone to centerline (E). In the adiabatic section, the radial velocity is zero. In the condenser section, the radial velocity increases from centerline (E) to near liquid-vapor interface (F) due to suction velocity. After this increase, the radial velocity decreases in two stages. The first stage decrease is from near liquid-vapor interface (F) to liquid-vapor interface (G) due to condensation. The second stage decrease is from liquid-vapor interface (G) to wall-liquid interface (A) due to heat released at the outer wall surface. These results are in good agreement with the earlier study [14], and radial temperature distribution shown in **Fig. 5**.

6.6. Statistical analysis of the temperature data

An analysis of the statistical differences between the present numerical result (axial outer wall temperature) and previous experimental results (axial outer wall temperature) was carried out by test of hypotheses using two-sample t -test method. This method is used to test of hypotheses because the number of samples is less than 30 and assuming variances from present results and previous experimental results is equal [26]. The hypotheses set up for present work were:

$$H_0 = \mu_1 - \mu_2 = 0 \quad (21)$$

$$H_A = \mu_1 - \mu_2 \neq 0 \quad (22)$$

The μ_1 represents the population mean of present numerical results, and μ_2 refers to population mean of previous experimental results. The test of these hypotheses was carried out by two-tail

t-test. If the result of two-sample *t*-test in absolute value is less than *t*-test reference, the H_0 is accepted [26]. The results of two-sample *t*-test and reference *t*-test in two tails are given as follows:

- The two-sample *t*-test of the temperature data is 0.42.
- Two-tails-*t*-test from *t*-test distribution table [26] at 99.5 % of confidence value and 24 degree freedom ($n_1 + n_2 - 2$) gives *t*-test in two-tails as ± 2.80 .
- The two-sample *t*-test is less than *t*-test from *t*-test distribution table ($0.42 < 2.80$).

This accepts null hypotheses and rejects alternative hypotheses and shows that the present results (the axial outer wall temperature) is not statistically different from previous experimental results at 99.5 % of confidence value and 0.01 level of significance.

7. Conclusions

The proposed model is formulated by non-Darcian transport to determine liquid flow in liquid-wick region. The mass flow rate per radian is used to describe inflow and outflow at liquid-vapor interface. The non-pure conduction heat transfer is used to describe heat transfer in liquid-wick zone and source terms of evaporation and condensation are added to liquid-wick zone to prevent the loss and gain in heat resulting in evaporation and condensation at liquid-vapor interface. The model gives the axial outer wall temperature profile, centerline velocity magnitude, centerline pressure and thermal performance of cylindrical heat pipe in circumferential heat which is in good agreement with theoretical investigation [2]. The present numerical model gives the results of axial outer wall temperature and velocity magnitude streamline that is better than previous numerical model [4,15,25]. The results of axial outer wall temperature are in a good agreement with experimental result [4]. The hypotheses test by two-sample *t*-test method between present results and previous experimental results for axial outer wall temperature is not statistically different from zero at 99.5 % of confidence and 0.01 of level of significance.

Acknowledgments

The CFD-RC commercial software made available by Department of Mechanical Engineering, Academic Division, Chulachomklao Royal Military Academy, Maung, Nakorn-Nayok, Thailand is acknowledged and appreciated.

Narong Pooyoo is grateful to National Science and Technology Development Agency (NSTDA), Thailand for financial support to conduct this research.

References

- [1] P. Maheshkumar, C. Muraleedharan, Experimental determination of entropy generation in flat heat pipes, *J. Mech. Eng. Res.* 4 (2012) 1–9.
- [2] J.P. Marshburn, Heat pipe investigation, Technical note, Goddard Space Flight Center, National Aeronautics and Space Administration, Washington, DC, 1973.
- [3] P.D. Dunn, D.A. Reay, *Heat Pipes, Theory Design and Applications*, Pergamon, New York, 2005.
- [4] A. Faghri, Analysis of frozen startup of high temperature heat pipes and three dimensional modeling, Interim Report for Period January 1990–May 1991, Aero Propulsion and Power directorate, Wright Laboratory, 1991.
- [5] H. Shabgard, A. Faghri, Performance characteristics of cylindrical heat pipes with multiple heat sources, *Appl. Therm. Eng.* 31 (2011) 3410–3418.
- [6] M. Aghvami, A. Faghri, Analysis of flat heat pipes with various heating and cooling configurations, *Appl. Therm. Eng.* 31 (2011) 2645–2655.
- [7] N. Zhu, K. Vafai, Analysis of cylindrical heat pipe incorporating the effects of liquid-vapor coupling and non-Darcian transport a closed form solution, *Int. J. Heat Mass Transfer* 42 (1999) 3405–3418.
- [8] A. Nouri-Borujerdi, M. Layeghi, A numerical analysis of vapor flow in concentric annular heat pipes, *J. Fluid Eng.* 126 (2004) 442–448.
- [9] S. Mahjoub, A. Mahtabrosham, Numerical simulation of a convectional heat pipe, *Proc. World Acad. Sci. Eng. Technol.* 29 (2008) 117–122.
- [10] N. Thuchayapong, A. Nakano, P. Sakulchangsatjatai, P. Terdton, Effect of capillary pressure on performance of a heat pipe: numerical approach with FEM, *Appl. Therm. Eng.* 32 (2012) 93–99.
- [11] M. Layeghi, A. Nouri-Borujerdi, Vapor flow analysis in partially-heated concentric annular heat pipes, *Int. J. Comput. Eng. Sci.* 5 (2004) 235–244.
- [12] A. Nouri-Borujerdi, M. Layeghi, Liquid flow analysis in concentric annular heat pipe wicks, *J. Porous Media* 8 (2005) 471–480.
- [13] A.S. Annamalai, V. Ramalingam, Experimental investigation and CFD analysis of an air cooled condenser heat pipe, *Therm. Sci.* 15 (2011) 757–772.
- [14] G.V. Kuzetsov, A.E. Sitnikov, Numerical modeling of heat and mass transfer in a low-temperature heat pipe, *J. Eng. Phys. Thermophys.* 75 (2002) 840–848.
- [15] T. Kaya, J. Goldak, Three-dimensional numerical analysis of heat and mass transfer in heat pipe, *Heat Mass Transfer* 43 (2007) 775–785.
- [16] S. de Ornelas, S. de Sousa, C. Dong, M. Fernelius, M. Hofer, T. Holsclaw, A. Jennison, D. Mai, K. Ninh, M. van der Poel, Mathematical Modeling, Numerical simulation and statistical optimization of heat pipe design, center for applied mathematics, computation and statistics, Department of Mathematics San Jose State University San Jose, CA, 2006.
- [17] P.R. Mistry, F.M. Thakkar, S. De, S. DasGupta, Indirect experimental validation of a two-dimensional model of the transient and steady-state characteristics of a wicked heat pipe, *Exp. Heat Transfer* 23 (2010) 333–348.
- [18] CFD-ACE+ V2009, CFD-ACE+ V2009 User Manual. ESI Group CFD, Incorporation, Atlanta, Georgia, 2009.
- [19] C. Xi, H. Peng, A note on the solution of conjugate heat transfer problems using SIMPLE-like algorithms, *Int. J. Heat Fluid Flow* 21 (2000) 463–467.
- [20] C.Y. Wang, P. Cheng, Multiphase flow and heat transfer in porous media, *Adv. Heat Transfer* 30 (1997) 93–182.
- [21] S. Ergun, Fluid flow through packed columns, *Chem. Eng. Program* 48 (1952) 89–90.
- [22] S.W. Chi, *Heat Pipe Theory and Practice*, McGraw-Hill, New York, 1976.
- [23] H.K. Versteeg, W. Malasekera, *An Introduction to Computational Fluid Dynamics the Finite Volume Method*, Pearson, Prentice hall, 2007.
- [24] G.P. Peterson, *Heat Pipes: Modeling, Testing and Applications*, John Wiley & Sons, Incorporation, United States of America, 1994.
- [25] J. Schmalhofer, A. Faghri, A study of circumferentially-heated and block-heated heat pipes-II, three-dimensional modeling as a conjugate problem, *Int. J. Heat Mass Transfer* 36 (1993) 213–226.
- [26] W. Ronald, M. Raymond, M. Sharoni, Y. Keying, *Probability & Statistics for Engineers & Scientist*, Pearson, Prentice hall, 2007.